# Calcitonin paracrine signaling controls atrial fibrogenesis and arrhythmia

Lucia M Moreira[1,15], Abhijit Takawale[2,8,15], Mohit Hulsurkar[3], David A Menassa[4,5], Agne Antanaviciute[13], Satadru K Lahiri[3], Neelam Mehta[1], Neil Evans[1], Constantinos Psarros[1], Paul Robinson[1], Alex Sparrow[1], Marc-Antoine Gillis[2], Neil Ashley[14], Patrice Naud[2], Javier Barallobre-Barreiro[12], Konstantinos Theofilatos[12], Angela Lee[1], Mary Norris[1], Michele V Clarke[7], Patricia K Russell[7], Barbara Casadei[1], Shoumo Bhattacharya[1], Jeffrey D Zajac[7], Rachel A Davey[7], Martin Sirois[2], Adam Mead[13], Alison Simmons[13], Manuel Mayr[12], Rana Sayeed[6], George Krasopoulos[6], Charles Redwood[1], Keith M Channon[1], Jean-Claude Tardif[2], Xander HT Wehrens[3], Stanley Nattel[2,8,9,10 *] and Svetlana Reilly[1 *].

[1] Division of Cardiovascular Medicine, Radcliffe Department of Medicine, British Heart Foundation Centre of Research Excellence, University of Oxford, John Radcliffe Hospital, Oxford, UK.

[2] Faculty of Medicine, Department of Pharmacology and Physiology, and Research Centre, Montreal Heart Institute and University of Montreal, Montreal, Quebec, Canada.

[3] Cardiovascular Research Institute, Departments of Molecular Physiology & Biophysics, Medicine, Baylor College of Medicine, Houston, TX, USA.

[4] Clinical Neurology, Nuffield Department of Clinical Neurosciences, University of Oxford, John Radcliffe Hospital, Oxford, UK.

[5] Biological Sciences, Faculty of Life and Environmental Sciences, University of Southampton, Highfield Campus, Southampton, UK.

[6] Cardiothoracic Surgery, Oxford Heart Centre, John Radcliffe Hospital, Oxford, UK.

[7] The Department of Medicine, Austin Health, The University of Melbourne, Heidelberg, Victoria, Australia, 3084.

[8] Department of Pharmacology and Therapeutics, McGill University, Montreal, Canada.

[9] Institute of Pharmacology, West German Heart and Vascular Center, University Duisburg-Essen, Germany.

[10] IHU LIRYC and Fondation Bordeaux Université, Bordeaux, France.

[12] King's British Heart Foundation Centre, King's College London, United Kingdom.

[13] Medical Research Council (MRC) Human Immunology Unit, MRC Weatherall Institute of Molecular Medicine (WIMM), University of Oxford, Oxford, OX3 9DS, UK

[14] Single-Cell Genomics Facility, Weatherall Institute of Molecular Medicine (WIMM), University of Oxford, UK.

[15] These authors contributed equally to this work.

[*] Shared senior authorship.

Corresponding author: svetlana.reilly@cardiov.ox.ac.uk

**Total word count** (excluding summary, references, methods and figure legends) is 2,592.

**Summary - Atrial fibrillation (AF), the most common cardiac arrhythmia, is a major contributor to population mortality and morbidity, particularly stroke-risk.[1] Atrial-tissue fibrosis is a central pathophysiological feature and hampers AF-treatment; the underlying molecular mechanisms are poorly understood and present therapies are inadequate.[2] Here, we show that calcitonin (CT), a well-recognized hormone product of the thyroid gland involved in bone metabolism,[3] is produced in significant quantities by atrial cardiomyocytes and acts in a paracrine fashion on neighbouring collagen-producing fibroblasts to control their proliferation and secretion of extracellular matrix proteins. Global disruption of CT-receptor signalling in mice causes atrial fibrosis and increases AF susceptibility. Atrial-specific knockdown (KD) of CT in atrial-targeted liver-kinase B1 (LKB1)-KD mice promotes atrial fibrosis and prolongs/increases the number of spontaneous AF-episodes, while atrial-specific CT overexpression prevents fibrosis and AF in LKB1-KD mice. Patients with persistent AF are characterised by six-**

**fold reduction in myocardial CT levels and by loss of fibroblast membrane CT receptors. Transcriptome analysis of human atrial fibroblasts exposed to CT show little change, whereas proteomic analysis indicates extensive alterations in extracellular-matrix proteins and pathways related to fibrogenesis, infection/immune responses and transcriptional regulation. Strategies to restore disrupted myocardial CT signalling may offer new therapeutic avenues for patients with AF.**

**Background –** AF, the most prevalent cardiac arrhythmia, is associated with significant mortality and morbidity. AF-treatment is complicated by adverse atrial remodelling[2]. Current pharmacological strategies for AF are non-specific and can produce adverse effects. The identification of novel pathophysiologically-related targets might open new therapeutic avenues[2].

AF-related structural remodelling involves accumulation of cross-linked collagen from atrial cardiofibroblasts (ACFs). The underlying mechanisms are incompletely understood. Calcitonin (CT), produced by thyroid parafollicular cells, plays a well-known role in bone resorption and collagen turnover[3], and affects other tissues like skeletal muscle.[4]

Circulating CT-levels decrease with age[5], the main risk-factor for AF.[1,2] Genome-wide-association studies (GWAS) report links between single-nucleotide polymorphisms in the CT-receptor (CTR) and body mass index[6], another AF risk-factor. CT prevents calcium-induced ventricular arrhythmias[7] and inhibits atrial chrono-/inotropic function[8]. No information is available about CT-involvement in AF, nor regarding functional extrathyroid CT-production.

Here, we sought to (i) assess whether atrial myocardium produces CT and identify the cellular source(s), (ii) explore paracrine CTR-mediated effects on ACF proliferation and

collagen processing and, (iii) determine whether CT-signalling regulates atrial fibrotic remodelling and AF-susceptibility.

## Results

**Atrial cardiomyocytes produce CT.** Atrial myocardium secretes several hormones[9]. We investigated CT gene-expression in human right-atrial tissue, isolated atrial cardiomyocytes (ACMs), ACFs and epicardial fat (detailed in **Extended Data Table 1**). Human CT originates from the calcitonin-related polypeptide-alpha (*CALCA*) gene on chromosome-11 (ID:ENSG00000110680), co-transcribed into alpha-calcitonin gene-related peptide (αCGRP). CT and αCGRP transcripts were detected in human atrium, isolated ACMs and ACFs, but not adipose tissue (**Fig.1a-c**). CT-protein was apparent in the secretome of human ACMs, but not ACFs (**Fig.1d**). Persistent-AF patients had impaired ability to produce mature CT and its precursor pro-CT (**Fig.1e-g**), mirrored by increased αCGRP-protein in human right-atrial tissue-lysates and ACM-secretome (**Extended Data Fig.1a-b**). ACM-CT and αCGRP mRNA-expression and CT/αCGRP ratio were unchanged in AF (**Extended Data Fig.1c-e**); ACM-CT correlated negatively with age (**Extended Data Fig.1f**). We then compared CT-gene expression and secretion between human ACMs and TT-cells (which constitutively produce large amounts of CT) from a 77-year old with medullary thyroid carcinoma. CT gene-expression in ACMs was ~half that of TT-cells (**Fig.1h**); ACM CT-secretion was ~16-fold greater than TT-cells (**Fig.1i**). Thus, human ACMs are an active source of extrathyroid CT.

**Human ACFs express functional CTRs**. CT exerts its biological actions via the CTR. Human atrial myocardium exclusively expresses the most abundant 1a-isoform of the CTR (**Extended Data Fig.1g-h)**. Similarly, CTRs are expressed in ACFs (by qPCR, immunoblotting and immunostaining; **Fig.1j-k, Extended Data Fig.1i**). CTR-activation by

CT caused time-dependent CTR translocation from cell-surface to cytoplasm (**Fig.1j**) and concentration-dependent changes in ACF morphology (by impedance-monitoring), **Extended Data Fig.1j**. CT concentration-dependently increased cyclic adenosine monophosphate (cAMP) in human ACFs (**Fig.1l**), an effect blocked by Gαs-, but not Gαi-, inhibition and prevented by the CTR-antagonist sCT8-32 (**Fig.1m**). The lack of CT-mediated changes in Erk1/2-phosphorylation (**Extended Data Fig.1k**) suggests absence of Gαq-mediated responses. Thus, human ACFs express a fully-functional CTR primarily coupled to Gαs.

**CT-CTR signaling regulates human ACF function *in vitro*.** Treatment (72-hour) of human ACFs with 100-nM CT produces a ~46% reduction in collagen accumulation with no changes in fibronectin (**Fig.2a**). CT-treated ACFs showed ~two-fold decrease in proliferation, cell migration and accumulation of calcium-enriched deposits (**Fig.2b-d**) with unchanged α-smooth muscle actin protein and mRNA (α-SMA; **Fig.2e-f**). CT-mediated effects on collagen-production and ACF-proliferation were reversed by silencing CTR with locked nucleic acid antisense oligonucleotides (**Fig.2g-h** and **Extended Data Fig.1l-m**). In TGFβ1-stimulated cells, 500-nM CT decreased cell migration (by ~42%), proliferation and secreted collagen (by ~40%) in ACFs (**Extended Data Fig.1r-s**). These results indicate that CT-CTR signaling actively inhibits collagen-1 production, ACF proliferation and migration.

While collagen accumulation and proliferation were inhibited by 100-nM CT, these were not altered by 10 and 100-nM αCGRP (for collagen) or 10-nM αCGRP (for proliferation; **Fig.2i-k** and **Extended Data Fig.1n-o**).

We next investigated whether CT affects collagen-1 synthesis, degradation and processing. CTR-activation with 72-hour exposure to 100-nM CT did not change the expression of fibrillar collagen-gene (**Extended Data Fig.2a-b**) or collagen-1 degradation marker C-terminal telopeptide (ICTP; **Extended Data Fig.2c-d**), but inhibited cleavage and processing

of pro-collagen into mature collagen alpha-2 chain (**Extended Data Fig.2e**). CT increased accumulation of unprocessed forms of collagen-1 (pro-collagen, collagen C-terminal pro-peptide and pC-collagen) and decreased formation of mature collagen-1. Bone morphogenetic protein type-1 (BMP1) cleaves pC-collagen[10]; we noted concentration-dependent CT-induced reductions in BMP1-activity without changes in BMP1 gene expression or protein (**Extended Data Fig.2f-h**). Stimulation of human ACFs with 500-nM CT for 72 hours did not affect collagen-1 gene-expression, but increased collagen-1 degradation (**Extended Data Fig.2i-j**). These results indicate that the inhibitory effects of CT on collagen-accumulation are, at least partly mediated via BMP1-inhibition and result from CT-interference with collagen processing and degradation rather than synthesis.

Human-ACF transcriptome (assessed by single-cell RNA-sequencing and microarrays) remained intact in ACFs cultured with 100-nM CT for 24 or 72 hours (**Extended Data Fig.2k-n** and **Source Data 1**), while CT significantly modified the ACF-proteome. CT suppressed accumulation of 143/191 fibrogenesis-related extracellular-matrix (ECM) proteins in human ACF-secretomes (collagen-1/-3 were among the most affected proteins; **Fig.3a-b** and **Source Data 2**), while altering 225/3253 cellular proteins (**Fig.3c** and **Source Data 3**). ACF secretion of selected non-ECM proteins was unaffected by CT (**Extended Data Fig.3a-d)**. The Gene Ontology (GO) analysis (**Fig.3d** and **Extended Data Fig.3e)** revealed cellular-protein enrichment for ribosomal pathway and biological processes/functions related to fibrogenesis (e.g., collagen-fibril organization, cadherin-binding and cell-adhesion), immune/infection responses and transcriptional regulation.

**Disrupted CT-CTR signaling in human ACFs in AF.** We next investigated whether CT can rescue the pro-fibrotic phenotype of AF-patient ACFs and whether AF is accompanied by changes in CTR protein-content, gene-expression or distribution. The protein-content and gene-expression of CTR were unchanged in postoperative and paroxysmal AF (**Extended**

**Data Fig.3f-i**); CTR protein, but not gene-expression, was modestly decreased in persistent-AF patients (**Extended Data Fig.3j-k**). Persistent-AF is typically accompanied by fibrosis,[11] but persistent-AF ACFs did not respond to CT, as CT did not affect collagen-1 production and cell-proliferation (scar-in-a-jar, **Fig.3e-f**), fibronectin production (scar-in-a-jar), ACF migration (scratch assay), or α-SMA protein (immunoblot), **Extended Data Fig.3l-m.**

Since the modest reduction in CTR-protein does not explain non-responsiveness to exogenous CT, we looked for endogenous AF-associated downstream signalling dysregulation or disease-related ACF-phenotype modification. ScRNA-seq (SMART-Seq2) of freshly-isolated human ACFs identified 5 transcriptional clusters (**Extended Data Fig.4a-c, e; Extended Data Fig.5** and **Source Data 4**). The largest cell-population (cluster-1) was abundant for ACTA2 and NOTCH3 transcripts typical of actively-proliferating myofibroblasts.[12] A smaller ACTA2-positive population (cluster-2) was enriched for myosins (e.g., MYH2, MYH3 and MYH7), representing cells with increased contractility that appear during wound-repair and contribute to ECM-stiffness.[13] Cluster-3 cells were ACTA2-negative (possibly embryonic fibroblasts, stellate cells or an intermediate cell-subset between fibroblasts and myofibroblasts).[14] $CD45^+$ (immature/leukocyte blood cell marker) and endothelial cells, incompletely depleted during ACF-isolation, formed clusters-4 and -5. Although clusters 2-5 were similar between SR and AF, the cluster-1 ACFs had 23 AF-associated deferentially-expressed genes (DEGs; **Extended Data Fig.4c-f** and **Source Data 5**) related to fundamental ACF-functions, including cell migration and invasion (RHOB), regulation of fibrogenesis (FOXF1, SIK1, NRF4A1, BHLHE40 and PDK4), differentiation (NR4A1, NR4A2, CEBP and SPC24), circadian rhythm (SIK1 and BHLHE40), metabolism (PDK4), immune-response/inflammation (IL6, ADAMTS1 and BHLHE40) and cell-transcription (NR4A1, NR4A2, BHLHE40 and FOXF1). Atrial protein-content of CT-CTR signalling components that may remain unchanged at the transcriptomic level. AF was

associated with increased expression of atrial cAMP (**Extended Data Fig.6a)**, a downstream mediator of CT-CTR (shown in **Fig.1l-m**).

In light of the limited change in CTR-expression in AF-ACFs, we verified CTR subcellular localisation. **Fig.3g** and **Extended Data Fig.6b** reveal that in persistent-AF ACFs, CTRs relocalise from cell-surfaces to intracellular spaces. Since CTR-responses require interaction with extracellular ligand, loss of cell-surface CTRs may be important in ACF non-responsiveness to CT in AF.

**Genetically-engineered CT-CTR dysfunction exacerbates atrial remodeling.** To assess AF-related consequences of depressed CTR-function, we assessed atrial fibrosis and AF-susceptibility in global CTR-KO and control heterozygous CTR-floxed mice.[15] CTR-KO mice showed significant atrial fibrosis (**Fig.4a-c**) with unchanged gene-expression of collagen-1 or -3, fibronectin and α-SMA (**Extended Data Fig.7a-d**) or cardiac morphology (**Fig.4a-**top panels). *In vivo* electrophysiological testing showed greater duration and inducibility of AF-episodes in CTR-KO mice versus controls (**Fig.4d-g** and **Extended Data Fig.7m-n)** with unchanged atrial effective refractory periods (**Fig.4h**), morphological parameters or hemodynamic function **(Extended Data Fig,7e-l** and **Extended Data Table 2a)**.

We next assessed the effect of ACM CT-production on AF-susceptibility. We modified an existing mouse model of spontaneous-AF, the LKB1-deficient mouse,[16] to produce atrial-specific knockdown (KD), and generated combined atrial-specific LKB1-KD/CT-overexpressing or LKB1-KD/CT-KD mice under the ANF promoter expressed in the cardiotropic adeno-associated vector AVV9[17] (**Fig.4i-k**). The atrial-specific LKB1-KD mice with reduced atrial CT levels (LKB1/CT-dKD, **Fig.4i-j**) had ~3.7-fold increase in atrial fibrosis (**Fig.4l-m**) with preserved cardiac structure and function (**Extended Data Table 2b**).

LKB1/CT-dKD mice developed spontaneous AF from 8 weeks of age, two weeks earlier than the LKB1-KD mice (**Fig.4n-o, r**). At 12 weeks, 62.5% of the LKB1/CT-dKD mice demonstrated spontaneous AF versus 23% of LKB1-KD mice (**Fig.4o, r**), and the AF episodes were ~16-fold longer in the LKB1/CT-dKD group (**Fig.4p**). CT overexpression in LKB1-KD murine atria prevented the spontaneous AF and atrial fibrosis observed in LKB1/CT-dKD mice (**Fig.4l-r**), reducing heart rate by 19% vs control $LKB1^{FL/FL}$ mice injected with lactated Ringer's solution (**Extended Data Table 2b**). These findings support the importance of CT-CTR signalling in AF arrhythmogenesis and atrial fibrotic remodeling.

**Discussion -** Here, we identified a new and significant role for CT, a CT-CTR signaling-cascade in human atrial myocardium that fine-tunes the function of ACFs to prevent excess fibrous-tissue accumulation (**Extended Data Fig.8a**). When this system becomes dysregulated, whether due to heart disease or CT/CTR gene-suppression, excess ACF-activity leads to collagen-accumulation and susceptibility to AF. Human ACMs represent a potent source of myocardial CT that exerts paracrine effects on ACFs by binding to ACF-CTRs, inhibiting cell-proliferation and fibrotic responses, in part via suppressed BMP1-dependent collagen-cleavage.

Atrial fibrosis, the most prominent feature of structural remodelling in AF, is commonly implicated in the arrhythmogenic substrate and is believed to be of great clinical pathophysiological and prognostic significance.[2,18] While many of the pathophysiological aspects of atrial fibrosis are understood[18], no clinically effective targets have yet been identified and there is a need to improve our mechanistic understanding to pinpoint novel mechanisms with the potential to lead to therapeutic breakthroughs.[2]

CT is primarily secreted by thyroid C-cells, yet thyroid agenesis or thyroidectomy do not consistently change circulating CT-concentrations,[19] pointing to substantial extra-thyroid

sources. Recent studies have uncovered extra-thyroid CT-secretion in human placenta[20] and sperm[21]. While no prior studies describe CT-synthesis in the heart, atrial myocardium is well-known to secrete a number of other hormones like atrial and brain natriuretic peptides, endothelin-1 and adrenomedullin. ACM CT-secretion was ~16-fold greater than that of the TT-cells we studied. Our findings raise the intriguing possibility that human atrial myocardium may represent a prominent source of CT and pro-CT, an important mediator and marker of inflammation that is widely used as a biomarker.[22] The physiological basis/function and regulation of pro-CT/CT production in the atrium requires further study. The atria are particularly prone to fibrosis, linked to hypersensitivity of ACFs to profibrotic stimuli[23], and the atrial CT-CTR axis might act as a counter-regulatory system. When cardiac pathology leads to an atrial fibrotic response, as in persistent AF, the diminished ACM CT-production and ACF membrane CTR-expression might, by removing the CT-CTR "brake" on the system, allow fibrosis to occur.

We found that ACFs from control patients express fully functional CTRs, coupled principally to Gαs-protein, consistent with prior observations of preferential CTR Gαs-coupling in other cell-types.[24] The CT-mediated increase in intracellular cAMP and the effect on collagen-1 accumulation and ACF proliferation were CTR-specific, as they were fully prevented by the CTR antagonist sCT8-32.[25] CT-mediated actions were independent of αCGRP, another splice-product of the *CALCA*-gene secreted by human ACMs, since exogenous αCGRP failed to alter human ACF collagen-production and proliferation. Discordant changes in ACM-CT and αCGRP levels might indicate preferential *CALCA* splicing towards αCGRP in persistent AF; this possibility requires further investigation.

The CT-induced decrease in ACF collagen-secretion might be caused by altered collagen synthesis, processing, and/or degradation. Our results show that low-concentration CT primarely inhibits maturation and cleavage of unprocessed collagen that is partly due to

decreased activity of BMP1, which cleaves the C-terminal pro-peptide of collagens 1-3[26] and is inhibited by increased intracellular cAMP[27]. CT stimulates ACF-cAMP production, which in turn plays a prominent role in cardiac fibrosis via downstream mediators including PKA and EPAC1/2[28]. Higher concentrations of CT accelerated collagen degradation in ACFs, suggesting that larger amounts of CT may influence multiple steps in collagen processing and be more effective in fibrosis suppression.

Unbiased high-throughput proteome-profiling of human ACFs revealed broad effects of CT on human ACFs, suggesting both direct ECM proteome-inhibition and effects on signalling controlling proliferation and migration. In ACFs from persistent-AF patients, CT failed to show antifibrotic actions, as CTRs were primarily localised in the ACF intracellular compartments in patients with AF, versus extensive cell-surface localisation in control-patient ACFs, precluding activation of membrane CTRs by extracellular CT. Whether the intracellular abundance of CTR in AF affects other ACF-functions remains to be explored. As AF-ACFs had unchanged CTR gene-expression and modestly-reduced CTR protein, defective CTR-processing and signalling (e.g., lack of CTR-chaperoning by an intracellular binding-protein like filamin-A,[29] or altered CTR trafficking by Receptor-Activity Modifying Proteins or RAMPs[30]) may be involved in disordered subcellular localisation. CTRs bound to RAMPs may respond to amylin and αCGRP.[30] Persistent AF also downregulated CT-CTR-cAMP axis effectors CREB and EPAC1 (which facilitate collagen-secretion and left-atrial fibrosis in HF[31]), possibly contributing to reduced anti-fibrotic effects in AF.

To test whether AF is associated with pre-existing transcriptional changes accounting for altered responses to CT, we performed single-cell scRNA-seq on freshly-isolated human ACFs. Non-cultured ACFs fell into 5 distinct transcriptional clusters, with AF-associated differential expression only present for $ACTA2^{+}NOTCH3^{+}$ cells. These cells show a profile associated with ACF migration/invasion, differentiation/transcription, fibrosis-regulation,

circadian rhythm and cellular immunity. These results reveal an additional level of complexity of AF-associated changes in ACFs that may underlie altered cellular responses, including those to CT.

The *in vivo* consequences of the disrupted CT-CTR signalling were tested in genetically modified mice. Global CTR gene-deletion enhanced atrial fibrosis in the absence of left atrial dilatation or left-ventricular dysfunction. To examine spontaneous AF-occurrence, we turned to a mouse model of LKB1-suppression. Myocardial-selective knockout of LKB1 involves effects secondary to ventricular LKB1-deletion.[16] Thus, we generated a novel atrial-specific LKB1-KD mouse model that developed spontaneous AF at 10 weeks of age without ventricular remodeling. CT-downregulation in the LKB1-KD mouse atria significantly worsened both arrhythmic and pro-fibrotic phenotype, with full rescue by atrial-targeted CT-overexpression.

**Conclusions** - We identified a novel CT-CTR paracrine signalling system in human atrium. Human ACMs represent a significant source of CT that, via binding to the CTR on the ACF membrane, controls fibroblast proliferation and BMP1-related collagen processing. Disruption of the CT-CTR axis permits excessive atrial fibrogenesis and promotes arrhythmogenesis. Restoration of the CT-CTR functional cascade might help to control the development of the AF-related arrhythmogenic substrate in man.

**REFERENCES.**


1. Chugh, S.S., *et al.* Worldwide epidemiology of atrial fibrillation: a Global Burden of Disease 2010 Study. *Circulation* 129, 837-847 (2014).
2. Heijman, J., Guichard, J.B., Dobrev, D. & Nattel, S. Translational Challenges in Atrial Fibrillation. *Circ Res* 122, 752-773 (2018).

3. Karsdal, M.A., Byrjalsen, I., Leeming, D.J., Delmas, P.D. & Christiansen, C. The effects of oral calcitonin on bone collagen maturation: implications for bone turnover and quality. *Osteoporos Int* 19, 1355-1361 (2008).
4. Yamaguchi, M.*, et al.* Calcitonin Receptor Signaling Inhibits Muscle Stem Cells from Escaping the Quiescent State and the Niche. *Cell Rep* 13, 302-314 (2015).
5. Basuyau, J.P., Mallet, E., Leroy, M. & Brunelle, P. Reference intervals for serum calcitonin in men, women, and children. *Clin Chem* 50, 1828-1830 (2004).
6. Locke, A.E.*, et al.* Genetic studies of body mass index yield new insights for obesity biology. *Nature* 518, 197-206 (2015).
7. Cuparencu, B., Ticsa, I., Barzu, T., Sandor, V. & Gozariu, L. [Effect of calcitonin on certain experimental models of arrhythmia]. *Therapie*, 555-563 (1975).
8. Chiba, S. & Himori, N. Effects of salmon calcitonin on SA nodal pacemaker activity and contractility in isolated, blood-perfused atrial and papillary muscle preparations of dogs. *Jpn Heart J* 18, 214-220 (1977).
9. Ogawa, T. & de Bold, A.J. The heart as an endocrine organ. *Endocr Connect* 3, R31-44 (2014).
10. Vadon-Le Goff, S., Hulmes, D.J. & Moali, C. BMP-1/tolloid-like proteinases synchronize matrix assembly with growth factor activation to promote morphogenesis and tissue remodeling. *Matrix Biol* 44-46, 14-23 (2015).
11. Martins, R.P.*, et al.* Dominant frequency increase rate predicts transition from paroxysmal to long-term persistent atrial fibrillation. *Circulation* 129, 1472-1482 (2014).
12. Grieskamp, T., Rudat, C., Ludtke, T.H., Norden, J. & Kispert, A. Notch signaling regulates smooth muscle differentiation of epicardium-derived cells. *Circ Res* 108, 813-823 (2011).

13. Bond, J.E., *et al.* Temporal spatial expression and function of non-muscle myosin II isoforms IIA and IIB in scar remodeling. *Lab Invest* 91, 499-508 (2011).
14. Li, H., *et al.* Reference component analysis of single-cell transcriptomes elucidates cellular heterogeneity in human colorectal tumors. *Nat Genet* 49, 708-718 (2017).
15. Davey, R.A., *et al.* Calcitonin receptor plays a physiological role to protect against hypercalcemia in mice. *J Bone Miner Res* 23, 1182-1193 (2008).
16. Ozcan, C., Battaglia, E., Young, R. & Suzuki, G. LKB1 knockout mouse develops spontaneous atrial fibrillation and provides mechanistic insights into human disease process. *J Am Heart Assoc* 4, e001733 (2015).
17. Ni, L., *et al.* Atrial-Specific Gene Delivery Using an Adeno-Associated Viral Vector. *Circ Res* 124, 256-262 (2019).
18. Nattel, S. Molecular and Cellular Mechanisms of Atrial Fibrosis in Atrial Fibrillation. *JACC Clin Electrophysiol* 3, 425-435 (2017).
19. Basuyau, J.P., Mallet, E., Leroy, M. & Brunelle, P. Reference intervals for serum calcitonin in men, women, and children. *Clin Chem* 50, 1828-1830 (2004).
20. Balabanova, S., Kruse, B. & Wolf, A.S. Calcitonin secretion by human placental tissue. *Acta Obstet Gynecol Scand* 66, 323-326 (1987).
21. Fraioli, F., *et al.* Beta-endorphin, Met-enkephalin, and calcitonin in human semen: evidence for a possible role in human sperm motility. *Ann N Y Acad Sci* 438, 365-370 (1984).
22. Schuetz P, Daniels LB, Kulkarni P, Anker SD, Mueller B. Procalcitonin: A new biomarker for the cardiologist. Int J Cardiol. 2016 Nov 15;223:390-397.
23. Burstein, B., Libby, E., Calderone, A. & Nattel, S. Differential behaviors of atrial versus ventricular fibroblasts: a potential role for platelet-derived growth factor in atrial-ventricular remodeling differences. *Circulation* 117, 1630-1641 (2008).

24. Andreassen, K.V., *et al.* Prolonged calcitonin receptor signaling by salmon, but not human calcitonin, reveals ligand bias. *PLoS One* 9, e92042 (2014).
25. Hay, D.L., Garelja, M.L., Poyner, D.R. & Walker, C.S. Update on the pharmacology of calcitonin/CGRP family of peptides: IUPHAR Review 25. *Br J Pharmacol* 175, 3-17 (2018).
26. Prockop, D.J., Sieron, A.L. & Li, S.W. Procollagen N-proteinase and procollagen C-proteinase. Two unusual metalloproteinases that are essential for procollagen processing probably have important roles in development and cell signaling. *Matrix Biol* 16, 399-408 (1998).
27. Zhang, S., Kaplan, F.S. & Shore, E.M. Different roles of GNAS and cAMP signaling during early and late stages of osteogenic differentiation. *Horm Metab Res* 44, 724-731 (2012).
28. Delaunay, M., Osman, H., Kaiser, S. & Diviani, D. The Role of Cyclic AMP Signaling in Cardiac Fibrosis. *Cells* 9(2019).
29. Nakamura, F., Song, M., Hartwig, J.H. & Stossel, T.P. Documentation and localization of force-mediated filamin A domain perturbations in moving cells. *Nat Commun* 5, 4656 (2014).
30. Hay, D.L., Christopoulos, G., Christopoulos, A., Poyner, D.R. & Sexton, P.M. Pharmacological discrimination of calcitonin receptor: receptor activity-modifying protein complexes. *Mol Pharmacol* **67**, 1655-1665 (2005).
31. Surinkaew, S., *et al.* Exchange protein activated by cyclic-adenosine monophosphate (Epac) regulates atrial fibroblast function and controls cardiac remodelling. *Cardiovasc Res* 115, 94-106 (2019).

**FIGURE LEGENDS.**

**Fig.1. Myocardial CT-production. a,** PCR-gel images in human atrial tissue, fibroblasts (ACFs), myocytes (ACMs), adipose-tissue and TT-cells; water and omitted reverse transcriptase (–RT) are negative controls. **b-c**, *CALCA* expression (qRT-PCR) in ACFs and ACMs. **d**, CT-secretion (cell-pellet, Pel; secretome, Sec). **e-f**, Pro-CT in atria (immunoblot; e) and ACM secretome (ELISA; f). **g**, ACM-secreted CT in patients with AF and sinus-rhythm controls (SR). **h-i**, *CALCA* expression and CT-secretion for human TT cells vs ACMs. **j,** Effect of CT on CTR-localisation in ACFs. **k**, CTR gene expression in ACFs. **l-m**, CT-effect on ACF cAMP, blocked by Gs-inhibitor NF499 or CTR-antagonist sCT8-32, not by Gi-inhibitor PTX. Data are mean±SEM, except for (f, g-i, l), median/interquartile-range; n, independent subjects. Two-sided tests: one-way ANOVA with Sidak's correction (d, m), unpaired t-test (e), Mann-Whitney (e, g-i), Kruskal-Wallis/Dunn's correction (l). Gel source-data in *Supplementary Figure 1;* replication-information in *Supplementary Information 1.17*.

**Fig.2. CT regulates human atrial cardiofibroblasts (ACFs). a**, Effect of 72-hour 100-nM CT on collagen-1 (green) and fibronectin (red) in ACFs (scale-0.3 mm; RFU, relative fluorescence units; DAPI (blue). **b-d**, CT inhibits cell-proliferation (b), calcium-enriched deposition (c) and cell-migration (d). **e-f**, Effect of CT on ACF α-smooth muscle actin (α-SMA) protein (e) and mRNA (*ACTA2*; f). **g-h**, Locked antisense nucleic acid oligonucleotide CTR-silencing (LNA-aCTR) blocks CT-effects on hydroxyproline-accumulation (HPA; g) and ACF-proliferation (h). **i-k**, Effect of 10-nM αCGRP on 24-hour ACF proliferation (i) and 72-hour collagen secretion (Sirius red) in conditioned medium without (j) or with 10 ng/ml TGFβ1 (k); BIBN4096 - CGRP receptor antagonist. Results are mean±SEM, except for: (a, h) median/interquartile-range; (c) mean±SD. Two-sided tests: Mann-Whitney (a), unpaired *t*-tests (e-f), two-way ANOVA with Sidak's correction (b, d), one-way ANOVA with Sidak's correction (c, g), Kruskal-Wallis/Dunn's correction (h) and Friedman test (i-k); n, individual

subjects; fc, fold-change. Gel source-data in *Supplementary Figure 1;* replication information in *Supplementary Information 1.17.*

**Fig.3. CT and physiology of ACFs. a-c,** Volcano-plots of differentially-expressed (DE) human ACF proteins after 72-hour treatment with 100-nM CT (significant changes colour-coded); violin-plots for top DE secreted proteins. **d**, Functional enrichment analysis of DE cellular proteins. **e-f,** CT-effects on ACF collagen-1 (e) and cell-proliferation (f; fc, fold-change) in persistent-AF. **g,** Immunofluorescence images of CTR (green) localisation in human ACFs from persistent-AF or sinus rhythm (SR). Similar results were obtained in 24 ACFs from 12 AF and 15 ACFs from 6 SR subjects. Data in (a-b) are adjusted for multiple testing with Benjamini-Hochberg false discovery rate (FDR) calculated by limma package v3.34.5 and Empirical Bayes (ebayes) algorithm, except in (c), p-values have not been corrected for multiple testing given that 3253 proteins were quantified. Functional enrichment analysis used DAVID 6.8 with human proteome background. Data in (e-f) are averages with interquartile ranges analysed by two-sided Kruskal-Wallis with Dunn's correction. Gel source-data in *Supplementary Figure 1;* replication information in *Supplementary Information 1.17.*

**Fig.4. CT-CTR signalling, atrial fibrosis and AF inducibility. a-c,** Masson Trichrome images of murine hearts (top) or atria (bottom), atrial fibrosis quantified in (b-c). **d-h**, Induced AF-episodes (d), AF-duration (e-f), AF-inducibility (g) and atrial effective refractory period (AERP) (h) in mice. **i-j,** Immunoblots (i) and quantification (j) of atrial protein normalised to GAPDH, as fold-change vs $LKB1^{FL/FL}$ control mice (fc). **k,** Constructs used; Inverted Terminal Repeats (ITRs, 145-nucleotide sequences) to generate capsidized AAV9 to integrate viral DNA between ITRs into host genomic DNA; modified ANF-promoter drives atrial-specific CRE (k-A) and CT(*Calca*)-cDNA; STOP sequence is flanked by lox-P sites (green arrows) cleaved under ANF-driven CRE to enable shRNA expression specifically

414 targeting CT/pro-CT, shCT(Calca (k-B); CT(*Calca*)-cDNA is driven by ANF-promoter,
415 followed by mCherry that is separated by T2A sequence, which cleaves CT protein from
416 mCherry (k-C). **l-m**, Masson Trichrome images of hearts (l-top) or atria (l-bottom); atrial
417 fibrosis quantified in (m). **n-r,** Recordings of spontaneous AF (n), AF-free survival (o) and
418 longest AF-duration (p) for depicted groups; animals at risk (**r**). n, individual animals. Data
419 are mean±SEM except in (c, f, j-pro-CT/j-pro-αCGRP; m and p), median/interquartile range.
420 Two-sided tests: unpaired *t*-test (b, h), Mann-Whitney (c, f), Kruskal-Wallis/Dunn's
421 correction (j-pro-CT/pro-αCGRP; m), log-rank (o), or one-way ANOVA/Holm-Sidak's (j-
422 αCGRP), Sidak's correction in (j-LKB1, j-CT-log-transformed, p-log-transformed); one-
423 sided Fisher's exact test (g). Gel source-data in *Supplementary Figure 1;* replication
424 information in *Supplementary Information 1.17*.

425 **MATERIALS AND METHODS**.

426 **Patient cohorts.** Studies involving human participants were approved by the local Research
427 Ethics Committee (South Central - Berkshire B Research Ethics Committee, UK; ref:
428 18/SC/0404 and 07/Q1607/38). All patients gave informed written consent. A total of 156
429 patients were included in the study; all patients underwent cardiac surgery (coronary artery
430 bypass grafting or valve repair/replacement) in the John Radcliffe hospital at Oxford.
431 Detailed patient characteristics are shown in **Extended Data Table 1**. Right atrial biopsies
432 were collected before cardiopulmonary bypass and immediately processed for cell isolation
433 (described below) or snap-frozen until use in other experiments (e.g., gene expression and
434 immunoblotting).

435 **Animal models.** All animal breeding, handling and experimental work were carried out in
436 three centres, Montreal Heart Institute (Canada), The Department of Medicine, Austin
437 Health, University of Melbourne (Australia) and the Baylor College of Medicine (Houston,
438 USA).

Global CTR-KO mice were generated as described previously[5]. Ten or twelve-week-old age and sex matched mice (121 in total) were used in all animal experiments. CTR-KO mice were compared to their control littermates (heterozygous CTR-floxed); females and males were analysed separately for some experiments (depicted in **Fig.4a-c** and **Extended Data Fif.7a-l**). All animal work was performed in accordance with the local (Montreal Heart Institute and Austin Health) Animal Care and Ethics Committee guidance and in accordance with NIH guidelines. The CTR-KO and control mice (Montreal cohort) were housed in Allentown XJ cages at 20-22°C, 50% humidity and 60 air changes/hour ventilation conditions. Diet consisted of the sterilized food (#2019S, Envigo) and osmotic water.

The CTR-KO and control mice (Melbourne cohort) were housed in a specified pathogen-free facility at 22°C, in a 12-hour light/dark cycle and were supplied with standard irradiated mouse chow (1.2% calcium and 0.96% phosphorus; Ridley Agriproducts, Western Australia) and water ad libitum. Breeding mice were housed in micro-isolator cages and offspring used for experiments were transferred to open-top cages at weaning (3–5 mice/cage). Cages contained corn-cob bedding, and cardboard tubes and tissues were supplied for environmental enrichment.

Studies in LKB1-KD, LKB1/CT-dKD, LKB1-KD+CT and controls (Houston cohort) were performed according to protocols approved by the Institutional Animal Care and Use Committee (IACUC) at the Baylor College of Medicine. All mice were housed in standard mice cages provided with the bags of sizzle net as cage enrichment and were fed standard feeder chow as approved by the IACUC and recommended by 'the Guide' (NIH Publication #85-23, revised 1996).

**Generation of LKB1/CT-KD and LKB1-KD+CT mice.** The $LKB1^{FL/FL}$ mice were purchased from Jackson Laboratory (#014143 - Lkb1fl; Jackson Laboratory, USA). The shRNA for murine *Calca* (TRCN0000184797; Sigma-Aldrich, USA) was embedded within a

miR-30a scaffold in an AAV9 vector containing Cre-recombinase gene under the regulation of ANF promoter to facilitate its transcription by Polymerase II (**Extended Data Fig.7l**). As described previously,[17] 5x $10^{10}$ genome containing units of AAV9 were diluted in lactated Ringer's solution and administered subcutaneously in 5 days old pups. Mice injected with equal volume of lactated Ringer's solution were used as negative controls. For the ease of identification, all the pups from one litter, one cage were injected with the same AAV9 or Ringer's solution and returned to the cages to be nursed. Mice were weaned at the age of 21 days and males-females were separated in to designated cages. A total number of 38 mice were used for the final experiments.

**Harvesting of the murine tissue.** Mice were weighed and anesthetized using isoflurane and euthanized via cervical dislocation. Hearts were extracted quickly and dipped once in clean saline solution to remove excess blood. For immunoblot and qPCR experiments, atria were separated from the ventricles. Left and right atria as well as ventricles were weighted, stored in respective tubes and flash frozen in liquid nitrogen. For histology, whole hearts were dipped into another container with clean saline solution (for Houston cohort) or arrested in diastole with 1M/L KCl (for Montreal cohort), fixed in 10% neutral buffered formalin (#HT501128; Sigma-Aldrich, USA) for at least 24 hours and embedded in paraffin.

**Isolation and culture of primary human ACFs.** Human ACFs were isolated and cultured from right atrial biopsies obtained from patients who underwent cardiac surgery. Tissue biopsies were cut into small (2-3 $mm^3$) pieces and repeatedly digested using 4 mg/ml collagenase II and trypsin (0.0625%). Cells were washed twice with sterile phosphate-buffered saline (PBS) and plated onto 6-well plates in FBM-3 medium (#CC-3131, Lonza, USA) containing 10% FBS and a supplement pack (#CC-4525, Lonza, USA) and kept in a humidified atmosphere at 37 °C and 5% CO2. The medium was renewed every 2–3 days. At ~80–90% confluence, cells were passaged using a standard trypsinisation method. For the

experiments with TGF-β1 stimulation, we used commercially available donors of human primary atrial fibroblasts (#CC-2903, Lonza, USA), which were maintained and cultured in the same medium as outlined above. Experiments were carried out at cell passages P3-4 and cells were cultured in serum-free media for ~16 h before intervention and treatment with 100 or 500-nM of human CT (#H-2250, Bachem, Switzerland), with 10-nM of human αCGRP (#3012, Tocris Bioscience, USA), 10-nM of BIBN4096 (#4561,Tocris Bioscience, USA), 100-nM of sCT8-32 (#4037182, Bachem, Switzerland) and 10- ng/ml of TGF-β1 (#HZ-1011, Proteintech, USA).

**Isolation and maintenance of primary human ACMs.** Right atrial cardiomyocytes (ACMs) were isolated using a standard enzymatic dispersion technique, as described previously[32] and detailed in *Supplementary Methods 1.1*.

**Sources of other human cells** are detailed in *Supplementary Methods 1.2*.

**Transfection of primary human ACFs.** Silencing of the CTR was carried out in ACFs transfected with 50 nM of antisense LNA™ (locked nucleic acid) oligonucleotides targeting CTR (#300600, Exiqon; design 1 - C*T*G*G*G*T*G*C*G*C*T*A*A*A*T*A and design 2 - A*T*G*A*C*A*T*A*G*A*T*G*A*G*A*C; LNA is not shown, as this information is proprietary), or antisense LNA™ oligonucleotides negative control A (#300610, Exiqon) using lipofectamine™ RNAiMAX transfection reagent (#13778075, ThermoFischer Scientific, USA) in antibiotic-deprived FBM-3 medium containing 2% FBS (both from Lonza and detailed above). Efficient knockdown was confirmed by the real-time qPCR and Western blot (**Extended Data Fig.1l-m)**.

**Western blot.** Immunoblotting is described in *Supplementary Methods 1.3*. The list of antibodies and validation of the anti-CTR/anti-pro-CT antibodies are shown in *Supplementary Table 1* and **Extended Data Fig.8b-g** respectively.

**Colorimetric assays.** Quantification of total secreted collagen in the cell culture supernatant was performed using a Sirius Red collagen detection kit (#9062, Chondrex Inc, USA) as previously described[33]. The levels of human CT in cell supernatant was quantified using ELISA (#CEA472Hu, Cloud-Clone Corp, USA) with the detection range of 12.35-1000 pg/ml and the lowest detectable level less than 4.74 pg/ml; experimental recovery of cellular secretome matrix was 98% on average. This kit did not show any cross-reactivity with αCGRP or pro-CT (**Extended Data Fig.8h-i**). Concentration of human pro-CT was measured by ELISA kit (#ab221828, Abcam, UK). Concentration of human αCGRP was measured by EIA kit (#A05481.96, BioVendor, BertinPharma, USA) with a detection limit < 10 pg/ml. The amount of total collagen in human ACFs was quantified by colorimetric detection of hydroxyproline using a Quickzyme total collagen assay kit (#QZBTOTCOL1, lot 0795, QuickZyme Biosciences). Quantification of the human collagen 1 C-terminal telopeptide (ICTP) was carried out using ELISA kit (#CSB-E10363h, Cusabio, USA).

Cyclic adenosine monophosphate (cAMP) was quantified using HitHunter cAMP Assay for Small Molecules kit (#90-0075SM2, DiscoverX-Eurofins, USA); cAMP was measured in the presence or absence of the selective inhibitor of Gαs protein NF499 (4,4',4",4'"-(carbonylbis(imino-5,1,3-benzenetriylbis(carbonylimino))) tetrakis-benzene-1,3-disulfonic acid[34]; 10 µM, #N4784, Sigma-Aldrich, USA), Gαi inhibitor pertussis toxin (PTX, 20 ng/ml, CAS #70323-44-3, Calbiochem, USA), human CT (100 nM, #H-2250, Bachem, Switzerland), CTR antagonist (salmon calcitonin sCT8-32, 100 nM, #4037182, Bachem, Switzerland) and cAMP activator forskolin (FSK, 100 µM, #1099, Tocris Bioscience, USA). Concentrations of the selected non-ECM proteins CTGF, CCL2, TNFα and IGF-II secreted by human ACFs treated with 100 nM CT for 72 hours were assessed by ELISA kits #DY9190-05, #DY279-05, #HSTA00E and #DY292-05 respectively (all from R&D Systems, UK).

All colorimetric assays were performed according to the manufacturer protocols.

Accumulation of calcium-rich deposits by fibroblasts was assessed with Alizarin Red S staining (#A5533, Sigma-Aldrich, USA) as detailed in *Supplementary Methods 1.4*.

**Immunostaining and imaging of human ACFs.** Immunostaining for CTR was carried out in human ACFs. Briefly, cells were fixed in precooled (−20°C) acetone/methanol (1:1) solution, air-dried and rinsed 3 times in PBS, blocked with serum-free blocking reagent (#X090930-2, DAKO, Agilent Technologies), and incubated with an anti-CTR and anti-filamin A (detailed in the Supplementary Table 1) antibodies overnight at 4°C. After multiple rinsing steps with PBS, secondary Alexa Fluor antibodies (Invitrogen) were applied for 2 hours at room temperature. Imaging was performed with a Zeiss LSM 710 or Leica DM 6000 CFS confocal imaging system. To assess cellular localisation of the CTR, optical sections of fibroblasts were imaged with a frame size of 157 μm x 157 μm at a z-depth of 1 μm and pixel resolution of 0.09 μm x 0.09 μm. Channels were subsequently split and then merged in Fiji open source software.

**BMP1 Enzyme Activity Assay.** BMP1 enzyme activity was measured with a fluorescent assay using fluorogenic substrate as detailed in *Supplementary Methods 1.5*.

**Scratch wound migration assay.** Human ACFs migration was determined using *in vitro* scratch wound assays on confluent monolayers of cells using chambers with 2 well silicone insert with a defined cell-free gap (#80206, Ibidi). Briefly, 5 x$10^3$ cells were seeded into each chamber in 70 μl of complete medium (with 10% FBS, as described above). When cells attached and reached ~95% confluency, they were synchronized in serum-free medium for 16 hours, which was followed by the chamber insert removal; cells were subjected to 24-hour treatment with 100-nM CT and/or 10 ng/ml TGFβ1. Changes in the wound area were imaged at 0 and 24 hours and quantified using ImageJ software.

**Scar-in-a-jar assay.** Collagen-1 accumulation by fibroblasts was assessed using a scar-in-a-jar assay detailed in *Supplementary Methods 1.6.*

**Assessment of cell proliferation.** Cell proliferation at a single time point was assessed by ELISA using BrDU (5-Bromo-2´-Deoxyuridine) DNA-binding probe (#QIA58, Calbiochem, Millipore, USA) according to the manufacturer's instructions. Briefly, human ACFs were plated in a sterile 96-well plate in a medium (FBM-3 #33-3131, Lonza, USA) containing 10% FBS and supplement pack (#CC-4525, Lonza, USA). Cells were incubated overnight with BrdU (kit component #JA1595) and fixed the next morning with the Fixative/Denaturing Solution (kit component #JA1598). Anti-BrdU antibody (kit component #JA1599) diluted 1:100 in antibody diluent (kit component #JA1604) was added in each well and incubated for 1 hour at room temperature, followed by three washes with a wash buffer (kit component #JA1617) before 30 minutes incubation of cells with peroxidase goat anti-mouse IgG (kit component #JA1618) reconstituted with conjugate diluent (kit component #JA1615) followed by three more washes with wash buffer and ionised water. Cells were then incubated for 15 min in the dark at room temperature with the substrate solution and then with the stop solution. Spectrophotometric detection was performed at a wavelength of 450 nm.

*Real-time proliferation* was measured using xCELLigence real-time cell analysis (RTCA) DP system (ACEA Biosciences Inc, USA) to monitor cell response in real-time mode, as previously described[34]. The latter setup was also used to record impedance to monitor CTR response to the ligand binding, as previously described. The data were analysed using the manufacturer's software RTCA DA v1.0.

**Real-time quantitative or non-quantitative Polymerase Chain Reaction (PCR).** Total RNA isolation, reverse transcription and (non)quantitative PCR are detailed in *Supplementary Methods 1.7*. Primer sequences and TaqMan assay IDs are listed in *Supplementary Table 3.*

**Histological assessment of cardiac fibrosis in mice.** Collagen content in murine hearts was assessed by Masson's trichrome staining and Picrosirius-Red as detailed in *Supplementary Methods 1.8.*

**Echocardiography of the murine heart.** Echocardiographic studies were performed as described previously[35] and detailed in in *Supplementary Methods 1.9.*

***In vivo* assessment of AF inducibility using trans-jugular electrostimulation in mice.** Assessment of susceptibility to AF was carried out in control (heterozygous CTR-floxed) and CTR-KO mice using iox2 software (v.2.8.0.13, EMKA technologies, FR). Mice were anaesthetized with isoflurane & oxygen mixture and positioned on temperature regulated operating table. Briefly, platinum electrodes were inserted into the limbs for ECG measurement & a 1.9 French Octapolar (Transonic) catheter was inserted into right jugular vein and positioned in the right atrium. After a baseline stable ECG recording, a twice pacing threshold rectangular stimulus pulses were obtained by multiprogrammable stimulator (ID). Atrial effective refractory period (ERP) was measured by delivering 7 (or 8) stimuli (S1) at fixed cycle length 100ms followed by one short coupled extra stimulation (S2) from 70 ms to 20 ms, with 2 ms decrement for precise atrial ERP estimation.

AF inducibility was determined with 50 Hz burst pacing for 3 seconds, with six bursts separated by 2 second interval; the cycle was repeated three times. AF was defied as a rapid, irregular atrial rhythm. Once AF was induced, pacing was immediately stopped to avoid interfering with the induced arrhythmias. AF duration was calculated as a mean duration of all induced AF episodes in each mouse. Surface ECG & catheter signals were recorded and analysed using iox2 software (v.2.8.0.13, EMKA technologies, FR). The experimenter was blinded to the genotype throughout the protocol and analysis.

**Surface ECG recording in mice.** Mice of 3-4 weeks of age (after gaining sufficient body size) were anaesthetised with isoflurane and placed on the Rodent Surgical Monitor with two

612 sets of Noninvasive ECG Electrodes (Indus Instruments, Webster, TX, USA) with animal
613 limbs being taped to the electrodes. Isoflurane was provided constantly through the nose cone
614 to ensure that the mouse remained asleep throughout the recording. The temperature of the
615 ECG board was adjusted in order to constantly maintain the body temperature (monitored by
616 a rectal temperature probe) in a range between $36.5^0$C and $37.5^0$C. The ECG tracing and
617 recordings were acquired for 20 minutes/mouse, minimum once a week, with the
618 IOX2.9.5.28 software (Emka Technologies, Paris, France). AF was defined by the absence of
619 p-waves and the irregularly irregular R-R intervals for a period of more than 10 seconds.

620 **Proteome profiling.**

621 ***(a) Processing of conditioned medium and de-glycosylation*** is conducted as previously
622 described[36] as detailed in *Supplementary Methods 1.10.*

623 ***(b) In-solution protein digestion and peptide clean-up*** is described in detail in
624 *Supplementary Methods 1.10.*

625 ***(c) Liquid chromatography and tandem mass spectrometry (LC-MS/MS).*** Cleaned peptides
626 were separated on a nanoflow LC system (Thermo Scientific Dionex UltiMate 3000
627 RSLCnano) as described in *Supplementary Methods 1.10.*

628 ***(d) Database search of LC-MS/MS data and data filtering*.** Proteome Discoverer software
629 (ThermoFisher Scientific, version 2.3.0.523) was used to search raw data files against a
630 hybrid human-bovine database (UniProtKB/Swiss-Prot version of January 2019) using
631 Mascot (Matrix Science, version 2.6.0) as described in *Supplementary Methods 1.10* and *1.16.*

632 **Flow Cytometry.** Human cultured or freshly isolated ACFs were sorted on a Becton
633 Dickinson (BD) FACS Aria Fusion III sorter using a 100 μm nozzle and FACSDiva software
634 v.8 (detailed in in *Supplementary Methods 1.11*).

**Singe-cell RNA-sequencing (scRNA-seq) of human ACFs.** Freshly isolated cells were used in SMART-Seq2 assay**,** while cultured ACFs were processed by a droplet-based 10x scRNA-seq.

***(a) SMART-Seq2 work flow.*** Freshly-isolated cells were resuspended in ice-cold PBS containing 3%-BSA, stained with DAPI and the viable singlets were sorted on a BD FACS Aria Fusion-III sorter (using FACSDiva v.8.0 software) into 96-well plates containing 4-µl SMART-Seq2 lysis buffer prior freezing at -80°C until needed for further processing. The released RNA was converted to cDNA and then sequence ready libraries as described (https://www.nature.com/articles/nprot. 2014.006), with minor modifications. ThermoFisher Superscript II reverse transcriptase and Roche Kapa PCR enzyme were substituted for Takara Smartscribe reverse transcriptase and SeqAmp PCR enzyme respectively. Twenty PCR cycles were used to amplify cDNA and Illumina Nextera XT kit was used to generate the sequence ready libraries. The 384 single cells were sequenced as a single pool on the Illumina Nextseq 500 system using a high out-put 75bp kit.

***(b) SMART-Seq2 scRNA-Seq Data Analysis.*** Raw SMART-Seq2 sequencing data were demultiplexed using Illumina bcl2fastq software (v.2.20.0.422) as described in detail in *Supplementary Methods 1.12* and *1.16.*

***(c) Droplet-based 10x scRNA-seq work flow.*** Cultured human ACFs were quickly and gently trypsinised and resuspended in ice-cold PBS containing 3% BSA, stained with DAPI and only viable singlets were sorted on a BD FACS Aria Fusion III sorter into individual low bind tubes. Cells were resuspended in 100 µl of staining buffer (3% BSA, 0.01% Tween and PBS), incubated with a serum-free blocking reagent (DAKO) for 10 minutes at 4˚C and labelled (20 minutes at 4˚C) with the unique Biolegend Total-seq A hashing antibodies (1 µg/mL, detailed in *Supplementary Table 2*) diluted in a staining buffer. After three washing steps with a staining buffer, cells were centrifuged at 4˚C for 5 minutes at 350 g and all

samples were merged at equal ratios in 1 ml of a staining buffer, centrifuged for 5 minutes at 350 g at 4˚C and resuspened in ice-cold PBS at ~ 1000 cells/µl and were immediately processed with a 10X Genomics Chromium B chip; cells were kept on ice through the whole procedure. The sample exome library was processed to a sequence ready library using the V3 3' Prime Gene Expression kit as per manufacturer's protocol. The hashing library was processed as per the hashing method Version: 2019-02-13 New York Genome Center Technology Innovation Lab (www.CITE-SEQ.com). Both libraries were pooled before sequencing on an Illumina Novaseq 6000.

***(d) Analysis of the droplet-based 10x scRNA-Seq data*.** Raw sequence reads were quality-checked using FastQC software (v.0.11.8, Andrews, 2010) using Human hg38 reference genome analysis set obtained from the University of California Santa Cruz (UCSC) ftp site (Kuhn, Haussler and Kent, 2013). Further details are described in *Supplementary Methods 1.13.*

***(d) Data analysis and sample demultiplexing of the droplet-based 10x scRNA-Seq data*.** Hashed samples were demultiplexed as described in detail in *Supplementary Methods 1.14 and 1.16*.

**Gene expression microarrays.**

Microarrays were performed on human ACFs treated with 100 nM CT or vehicle for 72 hours as described in *Supplementary Methods 1.15* and *1.16*.

**Statistical analysis.** Student's *t*-test was used in two-group comparisons of normally distributed data; normal distribution was assessed by Kolmogorov-Smirnov test. Multiple groups of normally distributed data of similar variance were compared by one-way or two-way ordinary or repeated measures ANOVA; for multiple comparisons, the Sidak's or Holm-Sidak's corrected P values are shown as appropriate. The Kruskal-Wallis or Mann-Whitney

*U* tests were used when the normality assumption was not met. Categorical variables were compared by one-sided Fisher's exact test. Age-CT relationship was analysed by Pearson's correlation test. Analysis of AF-free survival was performed using a log-rank (Mantel-Cox and Gehan-Breslow-Wilcoxon) tests applied to Kaplan–Meier survival curves. A value of $P < 0.05$ was considered statistically significant. Statistical analysis was performed using GraphPad Prism v7.05, v6.04, v8.02, or v8.04 software. Proteomic results were analysed as follows: each dataset was filtered to keep only the consistently quantified proteins defined as the ones with less than 30% missing values. All remaining missing values were imputed with KNN-Impute method using the default k value (k=3). The relative quantities of the proteins were scaled using log2 transformation. The limma package v3.34.5 has been used to compare between different phenotypes using the Ebayes algorithm and performing paired analysis when paired samples were available. The initial p-values were corrected for multiple testing using Benjamini-Hochberg false discovery rate (FDR) correction method. Functional enrichment analysis was conducted in a DAVID 6.8 web tool with the human proteome as background. The scRNA-seq datasets were analysed using R package software, as outlined in *Supplementary Methods 1.12. - 1.14*. A detailed list of the software packages is provided in *Supplementary Methods 1.16.*

**References associated with 'Methods'.**


32. Reilly, S.N., *et al*. Up-regulation of miR-31 in human atrial fibrillation begets the arrhythmia by depleting dystrophin and neuronal nitric oxide synthase. *Sci Transl Med* **8**, 340ra374 (2016).
33. Schafer, S., *et al.* IL-11 is a crucial determinant of cardiovascular fibrosis. *Nature* **552**, 110-115 (2017).
34. Hohenegger M et al. Gs alpha-selective G protein antagonists. Proc Natl Acad Sci U S A. 1998 Jan 6;95(1):346-51)

35. Alsina K.M., et al. Loss of Protein Phosphatase 1 Regulatory Subunit PPP1R3A Promotes Atrial Fibrillation. Circulation. 2019 Aug 20;140(8):681-693. doi: 10.1161/CIRCULATIONAHA.

36. Barallobre-Barreiro, J., *et al*. Extracellular matrix remodelling in response to venous hypertension: proteomics of human varicose veins. Cardiovasc Res. 2016 Jun 1;110(3):419-30. doi: 10.1093/cvr/cvw075.

**Data availability:** all data generated or analysed during this study are included in this published article. The scRNA-seq data are deposited on GEO at https://www.ncbi.nlm.nih.gov/geo/query/acc.cgi?acc=GSE148507 (ref: GSE148506, GSE148507 and GSE148504).

**Acknowledgments:** We thank the Oxford Genomics Centre at the Wellcome Centre for Human Genetics (funded by Wellcome Trust grant reference 203141/Z/16/Z) for the generation and initial processing of the ACF microarrays data; Prof Martin Farrall for the help with statistics; Kevin Clark in the WIMM Flow Cytometry Facility for his help; Dr Janet Digby for the assistance in conducting and analysis and detection of CT by ELISA in human ACFs and ACMs; Chantal St-Cyr - for managing, handling, genotyping mouse colonies and harvesting murine tissue samples at Montreal site; Dr Rody Hiram - for the initial help with the EP analysis in mice; Dr Jennifer Dewing - for creating an artistic sketch-summary of the main findings; Mr Lukas Emanuel Schmidt and Dr Xiaoke Yin - for their help with the proteomic experiments; Mr Shakil Farid and Mr Vivek Srivastava for their help with collection of some human atrial specimens during revision; Dr Peter Wookey - for his advice on the CTR protein detection; Dr Rohan Wijesurendra and Dr Parag Gajendragadkar - for the initial help in consenting patients for the study; Dr Alice Recalde and Maria C Carena - for the initial help with optimising fibroblast isolation protocol.

**Author contributions:** S.R. and S.N. conceived the study, designed the experiments, wrote and edited the manuscript. L.M.M. and A.T. wrote some parts of the manuscript, carried out and analysed most of the experimental work. K.M.C. provided intellectual input on the experiments in clinical samples. N.E., P.R., A.S. and C.R. performed some PCR, ELISAs and HPA measurements in human samples. Imaging and analysis of the CTR cellular localisation in human ACFs and HEK293 cells was performed by D.M. and L.M.M. All in vivo work in mice was carried out by A.T., M. H. and S.L., and supervised by X.H.T.W and S.N. Staining, imaging and analysis of fibrosis in murine heart sections was carried out by A.T., M. H., S.L. and C.P.; M.S. provided full access and supervision of the histological and imaging experiments at Montreal site. Primers design and gene expression assays in mice were carried out by P.N. and M.H.; primers design for human transcripts was performed by N.E., L.M.M. and C.P. Functional electrophysiological studies in CTR-KO mice were carried out by M.A. and A.T., and supervised by S.N.; echocardiography in CTR-KO mice was supported by J.C.T. The CTR-KO mice were generated and provided by J.D.Z. and R.A.D., who supervised murine tissue collection, genotyping and analysis of the selected morphologic parameters carried out by M.V.C. and P.K.R in Melbourne. All experimental work and data analysis in the LKB1-based mice was carried out by M.H and S.L., and supervised by X.H.T.W. Experiments in human cells were done by L.M.M., N.M. and N.E. The proteomic study was designed, executed and analysed by J.B.B. and K.T. under the supervision of M.M. Transcriptome profiling by scRNA-seq, performed by N.A., L.M.M and N.M., was designed and supervised by A.M. and S.R. Bioinformatic analysis of scRNA-seq results was carried out by A.A. and supervised by A.S. Scar-in-a-jar assay and analysis was carried out by A.L., supervised by S.B. Patients were consented by N.M., L.M.M. and M.N.; human atrial biopsies were collected by cardiac surgeons R.S. and G.K. under ethical approval granted to

B.C. and S.R. All authors discussed the results and had the opportunity to comment on the manuscript.

**Disclosures:** the authors declare no competing interests.

**Supplementary Information** is available for this paper.

**Funding Sources:** This study was funded by the British Heart Foundation (BHF) Intermediate Fellowship in Basic Science, by the Oxford BHF Centre of Research Excellence (CRE; RG/13/1/30181) Transitional Fellowship, BHF CRE Overseas Collaboration Travel award, the Medical Science Division Internal Fund, the Wellcome Trust Institutional Strategic Support Fund, the Oxfordshire Health Services Research Committee, the National Institute for Health (NIHR) Oxford Biomedical Research Centre and LAB282 grants (to S.R.); BHF Chair award CH/16/1/32013 (to K.M.C); by Canadian Institutes of Health Research (CIHR) and Heart and Stroke Foundation of Canada (to S.N.) and Fonds de Recherche en Santé de Québec (FRQS) & CIHR post-doctoral fellowships to A.T.

**Correspondence and requests** for materials should be addressed to S.R. and S.N.

**Extended Data figure legends and Extended Data table titles.**

**Extended Data Fig. 1. Effects of human αCGRP on human ACF function. a,** Secretion of αCGRP (ELISA) by human ACMs vs TT cells. **b**, αCGRP protein (immunoblot) in human right atrial tissue lysates obtained from patients with SR or AF. **c-e**, mRNA of human ACM CT, αCGRP or CT/αCGRP ratio between SR and AF groups. **f**, Correlation between donors' age and ACM-CT secretion (ELISA over 4-6 hours); 95%CI = -0.7912 to 0.01258, R = -0.4862, $R^2$ = 0.236, P = 0.056 by Pearson's correlation test. **g-i**, Human atrial myocardium (g) expresses CTR 1a, but not 1b, isoform (PCR using specific isoform primers) and CTR protein (h; TT cells - positive control, see Extended Data Fig. 8a); CTR protein content in ACFs (i). **j**, Representative traces (real-time impedance assay) showing CT-induced concentration-dependent increase of the baseline normalized cell index (CI). **k,** Total and

phosphorylated ERK was not altered by CT (immunoblitting). **l-m**, CTR mRNA (qRT-PCR) and protein content (immunoblotting) are decreased in the CTR knockdown human ACFs with LNA antisense oligonucleotides (designs LNA-aCTR1 and LNA-aCTR2); fc, fold change of the CTR-NC control. **n,** Effect of 10 and 100 nM αCGRP on 72-hour collagen accumulation (by Sirius red) in ACF secretomes. **o-r**, Effect of 100-nM CT on human ACF stimulated with TGFβ1 (10-ng/ml) on cell migration (o; fc, fold change of vehicle at 0 hours), collagen content in conditioned media (p) and cell proliferation (r). **s,** Representative blots (left) and quantification (right) of collagen-1 (Col1) in human ACF cell lysates and secretomes; n, indicates individual subjects; fc - fold of control. Data are presented as mean±SEM except for (a, b-Pro-αCGRP, c-e, k, s-panels 3/4, m), medians and interquartile ranges, (n), mean with paired scattered dots, and (o), mean±SD. P-values were determined by two-sided tests: unpaired *t* test (b- αCGRP, p-r), Mann-Whitney *U* test (b-Pro-αCGRP, c-e), Friedman test (n, s-panels 2/3) and Kruskal-Wallis with Dunn's correction (a, k) and repeated-measures one-way ANOVA with Sidak's correction (l, o, s-panels 1/4). Data are pooled from individual donors assessed in single replicates (a, b, f, g-k, m, o-s) or duplicates (c-e, l, n); all results were reproduced independently twice. For gel source data, see *Supplementary Figure 1*.

**Extended Data Fig. 2. Effect of CT on collagen-1 processing and single-cell transcriptome (10x scRNA-seq) of cultured human ACFs. a-d**, Effect of CT on collagen-1 in (a), collagen-3 in (b) synthesis (by qRT-qPCR), extracellular (c) and intracellular (d) content of collagen-1 C-terminal telopeptide (ICTP). **e,** Representative blots (left panel) and quantification (right panel) of unprocessed collagen-1 (pro-collagen, pro-Col and pC-collagen, pc-Col) and processed collagen-1 (Col 1) in human ACFs treated with 100 nM CT (fc, fold change of vehicle). **f-h,** Effect of exogenous CT on bone morphogenetic protein 1 (f; BMP1, immunoblotting), BPM1 gene expression (g; qRT-PCR) and on BMP1 activity (h) in

807 the presence or absence of BMP1 inhibitor (BMP1 inh; RFU, relative fluorescence units). **i-j**,
808 Effect of 24-hour 500-nM CT on collagen-1 (*Col1A1*) mRNA (qRT-PCR) and C-terminal
809 telopeptide (ICTP by ELISA). Data are mean±SEM, except (b, g, j), medians with
810 interquartile ranges; n, individual subjects. Two-sided tests: unpaired *t* test (a, c-f, i), Mann-
811 Whitney *U* (b, g, j) and one-way ANOVA with Sidak's correction (h). Data are pooled from
812 individual donor cells assessed in single replicates, except duplicates (a-b, g, i), on the same
813 day in one batch. Results were reproduced twice (a-c, f-h) in different donors. For gel source
814 data, see *Supplementary Figure 1*. **l-o**, Unbiased transcriptional clustering of scRNA-seq
815 data from human ACFs cultured with 100-nM CT for 24 hours or vehicle; demultiplexed by
816 final cell count per hash-tag in (l), transcriptional clusters in (m), pharmacological
817 intervention in (n) and by each donor in (o); D1-6, indicates individual donor. Active cycling
818 cells are pointed by arrow. All data are colour-coded within the figure. Data are pooled from
819 6 individual donors in sinus rhythm assessed in 14742 cells (post QC after filtering the initial
820 18466 total cellular barcodes) on the same day in one batch. tSNE, t stochastic neighbour
821 embedding; UMAP, Uniform Manifold Approximation and Projection.
822 **Extended Data Fig. 3. CTR expression and CT-mediated changes in ACF**. **a-d**, Effect of
823 72-hour 100 nM CT-treatment on IGF-II, CCL2, CTGF and TNFα in human ACF
824 conditioned media. Data are pooled from individual donor cells assessed on the same day in
825 technical duplicates, repeated twice; n, individual donors. P values were calculated by two-
826 sided tests: paired *t* test (a-c) and Wilcoxon test (d). **e**, GO enrichment analysis (David 6.8
827 web-tool) of the differentially expressed proteins under the above GO-terms stratified by
828 adjusted p-values. The bold number next to each term represents a number of genes under
829 each GO-term. The original data used for this analysis were pooled from 6 individual donors
830 treated with vehicle or 72-hour 100-nM CT assessed in single replicates on the same day in
831 one batch**. f-k**, Representative blots of the CTR protein and gene expression (qPCR) in

human AF-ACFs vs sinus rhythm (SR). **l-n**, Effects of CT-treatment of persistent-AF ACFs on fibronectin (l), α-SMA protein (m) and cell migration (n) by scratch wound assay (fc, fold-change) and. Data are mean±SEM, except (l, n) expressed as medians with interquartile ranges; (a-d) are shown as means and linked paired samples; n, individual subjects. P-values were determined by two-sided: paired t test (a-c), unpaired *t* test (f-k, m), Wilcoxon test (d), Mann-Whitney U test (n), and Kruskal-Wallis with Dunn's correction (l). Data are pooled from individual donors (l), or separate days (m-n) and assessed in single replicates on the same day in one batch apart from (n, single replicates on two different days), or in duplicates in (g, i, k) assessed on the same day. Findings in (a-d, j) were validated by another method (Fig.3a-b, g, Extended Data Fig.6b). All (except e) were reproduced twice in different donors. For gel source data, see *Supplementary Figure 1*.

**Extended Data Fig. 4. Single-cell transcriptome of freshly isolated human ACFs (scRNA-seq SMART-Seq2). a-b,** Transcriptional clustering (a) of freshly-isolated human ACFs stratified by donors in (b) labelled on the graph as SR1-4 or AF1-4. **c-f**, Differentially expressed genes (DEGs) in transcriptional cluster-1 (c, d, f) and volcano plots for clusters 2-5 are shown in (e; also see Source Data 5 and 6). P-values for DEGs were calculated by a log likelihood ratio test on a hurdle model (MAST framework tool) and have been corrected for multiple testing using Benjamini-Hochberg (see *Supplementary Methods 1.12 and 1.16*). Data are pooled from 268 single cells isolated from 8 individual donors; scRNA-seq workflow was performed on the same day in one batch.

**Extended Data Fig. 5. Cluster-comparison of single-cell transcriptome (SMART-Seq2) of freshly isolated human ACFs. a,** Transcriptional clustering of human ACFs (post QC) pooled from 4 individual donors in sinus rhythm (SR) and 4 individual donors in AF; figure shows the top 10 most abundant genes in each cluster. **b**, Gene Ontology (GO) functional enrichment analysis for human ACF transcriptional clusters. The number of significantly

857 enriched genes is shown within the figure. The p-values for GO panels are generated from a
858 hypergeometric distribution with a Benjamini-Hochberg correction. The original data are
859 pooled from 268 single cells isolated from 8 individual donors; the scRNA-seq workflow is
860 carried out on the same day in one batch.

861 **Extended Data Fig.6. Protein profiling of the selected CT-CTR downstream targets. a,**
862 Representative blots showing atrial protein content of BMP1, PKA subunit C (PKAC), PKA
863 subunit R2 (PKAR2), EPAC2, EPAC1, CREB and cAMP in AF (4 individual donors) vs 5
864 individual control donors in sinus rhythm (SR) group. All, but CREB, proteins were assessed
865 in the same membrane after protein stripping; all proteins are normalised to GAPDH and
866 expressed as fold of SR-control (fc); the red dotted line indicates y axis value of 1; n,
867 individual donors. Data are presented as medians with interquartile ranges. P-values were
868 determined by two-sided Mann-Whitney *U* test between SR and AF groups for each protein.
869 Data are pooled from individual donors assessed in single replicate on the same day; results
870 were reproduced in the same donors twice. For gel source data, see *Supplementary Figures*.
871 **b**, Immunofluorescence staining shows predominantly intracellular localisation of the CTRs
872 (green) in ACFs obtained from patients with persistent AF. By contrast, in SR-ACFs, the
873 CTR is localised to the cell-surface. Cells were counter-stained with filamin A (red) and
874 nuclei (DAPI). Data are pooled from the individual donors (a few cells in each field as shown
875 in the figure) collected over two-year period, assessed on separate days and validated by 3
876 independent experimenters. For source data please see *Supplementary Figure 1*.

877 **Extended Data Fig. 7. Atrial gene expression, morphological parameters and AF-**
878 **duration in mice. a-d**, Global CTR gene deletion does not alter atrial gene expression of
879 collagen 1 (*Col1A1*), collagen 3 (*Col3A1*), fibronectin (*Fn*) and alpha smooth muscle actin
880 (*ACTA2*) in male and female mice. **e-l**, Selected morphological parameters in the CTR-KO
881 males and females. **m-n**, Mean AF-duration in CTR-KO and control mice expressed as '*mean*

882 *of all AF episodes in mice who induced AF*' (m) or, as '*mean of all AF episodes in all mice*'
883 (n). **l**, Schematic representation of the constructs used to generate atrial-specific LKB1-KD,
884 LKB1/CT-dKD and LKB1-KD+CT mice. The LKB1FL/FL mice were injected with AAV9-
885 ANF-CRE. Since the ANF promoter drives expression of CRE exclusively in the atria, LKB1
886 was downregulated only in the atria of these LKB1-KD mice. The LKB1-KD+CT cDNA
887 mice received AAV9-ANF-CRE + AAV9-ANF-CT cDNA injections. Under ANF promoter,
888 CT was overexpressed exclusively in the atria of these mice. The LKB1/CT dKD mice
889 received AAV9-ANF-CRE + AAV9-loxP-STOP-loxP-shCT injections. Both, LKB1 and
890 LoxP-STOP-LoxP were deleted by atrial specific Cre enzyme, which allowed the expression
891 of CT shRNA, which selectively targets CT/pro-CT and not αCGRP sequence, and resulted
892 in the downregulation of both LKB1 and CT. Data are presented as mean values±SEM,
893 except (d-females, g-males, j and m-n), medians with interquartile ranges. P-values were
894 determined by two-sided tests: unpaired *t* test in all apart from (d-females, g-males, j, m-n) by
895 Mann-Whitney *U* test; n, indicates individual animals. Data are pooled from individual
896 animals assessed in single replicates on the same day and reproduced in two centres in (a, c-
897 d). Results in (m-n) were obtained from individual animals over ~2.5 years.
898 **Extended Data Fig. 8. Validation of anti-CTR antibody and study summary. a,** Data
899 summary: under physiological conditions in sinus rhythm (left panel), human atrial
900 cardiomyocytes produce and excrete endogenous CT, which binds to the CTR of atrial
901 cardiofibroblasts (ACFs). Increased Gs-mediated cAMP inhibits multiple steps of
902 fibrogenesis including, but not limited to, BMP1 activity and collagen processing by ACFs;
903 thus, keeping atrial fibrosis in check. In persistent AF (right panel), atrial cardiomyocytes
904 secrete less CT and ACFs show abnormal intracellular CTR localisation; the consequent
905 reduced CT-CTR activation enables unchecked structural remodelling and fibrosis in the atria
906 that promotes AF maintenance and inducibility. **b,** Immunostaining with anti-CTR antibody

907 shows barely detectable signal for CTR (green) in human kidney embryonic cell line
908 (HEK293) and adult human dermal fibroblasts (HDF), and prominent positive CTR staining
909 in human medullary carcinoma (TT) cells; filamin A (red) and nuclei (DAPI). Negative
910 control for secondary antibodies (with primary antibodies omitted) in human ACFs is shown.
911 **c**, Detection of positive immunofluorescence staining (green) with anti-CTR antibody in
912 control ACFs, but not in CTR-KD ACFs using anti-CTR LNA-antisense oligonucleotides. **d-**
913 **f**, The same antibody was used to detect CTR in HEK293 cells stably overexpressing
914 (+hCTR; confirmed by qRT-PCR) human CTR protein (d) by flow cytometry (e; control cells
915 negative for CTR (left plot) were used to determine the position of the P2 gate and the CTR+
916 cells (right plot) were sorted based on this gate and an antibody for CTR bound to AF647), or
917 by immunofluorescence (f; CTR+ cells are stained in green and nuclei, with DAPI, in blue).
918 Gating strategy shown (bottom 3 panels): cells were first gated by general size and
919 granularity (left plot), then doublets were excluded using a standard forward scatter height vs
920 area plot (middle plot), eliminating cells with a large area for any given signal height, and
921 then plotted on a log scale for mean fluorescent intensity of AF647 (right plot, gate P2) for
922 CTR+cells. The P2 gate was set based on unstained cells and shows events from the sample
923 with a mean fluorescent intensity higher than the control in P2 gate. **g,** Validation of the
924 antibody for human pro-CT in human atrial tissue by immunoblotting. Representative
925 example of the blot performed on 4 individual donors assessed in one day; this antibody was
926 also tested in another 4 individual donors on a different day with the same result;
927 recombinant human pro-CT was used as a positive control. **h-i**, CT-ELISA kit confirms
928 detection of human recombinant (in black) or synthetic CT (in green) in concentration-
929 dependent manner with no cross-reactivity with the recombinant human αCGRP or
930 recombinant human pro-CT (in magenta) at serial dilutions. **j**, Cellular pellets in proteomic
931 experiments were processed in duplicates to validate reproducibility. Data in (e) are presented

as medians with interquartile ranges analysed by two-sided unpaired *t* test after log-transformation. FSC-A, forward scatter area. Data in (b-d) are representative images of cells stained on the same day and reproduced three times on three separate days. Data are pooled from individual cultures assessed in duplicates (e), or from technical triplicates (h-i) and technical diplicates (j) analysed on the same day. For gel source data, see *Supplementary Figure 1*.

**Extended Data Table 1. Clinical characteristics of the study participants.** ACEI, angiotensin-converting enzyme inhibitor; ARB, angiotensin II receptor blocker; AVR, aortic valve replacement; CABG, coronary artery bypass surgery; COPD, chronic obstructive pulmonary disease; MI, myocardial infarction; MVR, mitral valve replacement. The one-sided Fisher's exact test was use to compare gender, surgical procedures, smoking status and medical history between groups. The two-sided unpaired *t* test was used to compare age. Percentage in parenthesis (%) indicates percentage within the same group (e.g., SR or AF). Characteristics of the participants used in scRNA-seq SMART-Seq2 experiment are shown in columns 10-12.

**Extended Data Table 2. *In vivo* echocardiographic and haemodynamic parameters in mice.** A - transmitral flow atrial filling; a‘ - mitral annulus moving velocity during atrial filling; CO - cardiac output; E - transmitral flow early filling; e‘ - mitral annulus moving velocity during early filling; EF - ejection fraction + (LVVd - LVVs)/LVVd X 100; FS - fractional shortening = (LADs – LADd)/LADs X 100; FS - fractional shortening = (LVDd - LVDs)/LVDd X 100; HR - heart rate; LV – left ventricle; LADd - left atrial dimension at end cardiac diastole; LADs - left atrial dimension at end cardiac systole; LV - left ventricle; LVDd - LV dimension at end cardiac diastole; LVAWd - LV anterior wall thickness at end cardiac diastole; LVIDd - LV internal diameter at diastole; LVIDd - LV internal dLVAWs - LV anterior wall thickness at end of cardiac systole; diameter at systole; LVPWd - LV

957 posterior wall thickness at end cardiac diastole; LVPWs- LV posterior wall thickness at end
958 of cardiac systole; LVDd - LV diameter systole; LVDs - LV dimension at end cardiac
959 systole; LVVd - LV volume at end cardiac diastole; LVVs - LV volume at end cardiac
960 systole; SV - stroke volume. Data in (a) were analysed by two-sided unpaired *t* test or Mann-
961 Whitney *U* test as appropriate; data in (b) were analysed by two-sided tests: one-way
962 ANOVA with Holm-Sidak's correction, except for LVAWd which was analysed by Kruskal-
963 Wallis with Dunn's correction test.

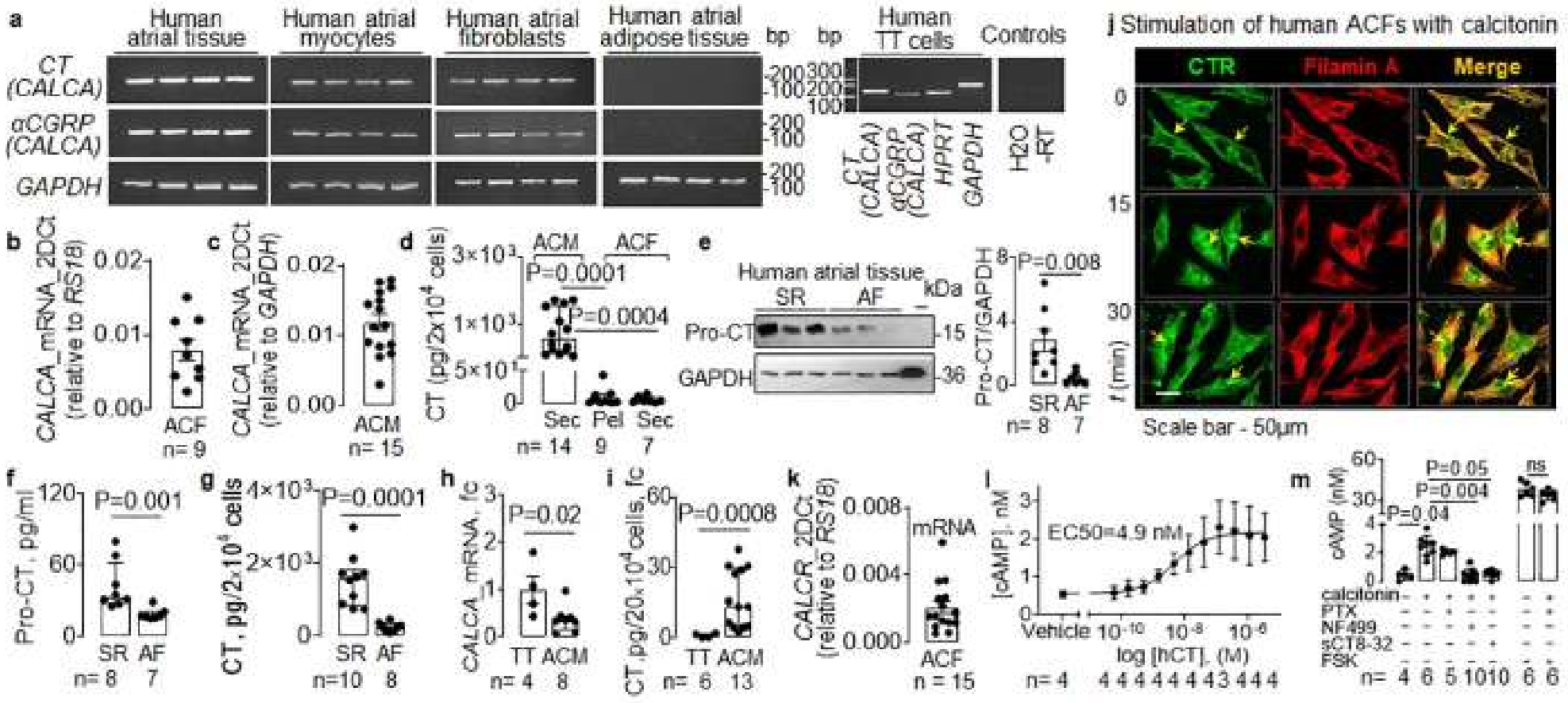
a
Human atrial tissue
Human atrial myocytes
Human atrial fibroblasts
Human atrial adipose tissue
bp
bp
Human TT cells
Controls
CT (CALCA)
αCGRP (CALCA)
GAPDH
HPRT
H2O
-RT
j Stimulation of human ACFs with calcitonin
CTR
Filamin A
Merge
0
15
30
t (min)
Scale bar - 50µm
b
CALCA_mRNA_2DCt (relative to RS18)
ACF
n= 9
c
CALCA_mRNA_2DCt (relative to GAPDH)
ACM
n= 15
d
CT (pg/2x10^4 cells)
ACM
ACF
P=0.0001
P=0.0004
Sec
Pel
Sec
n= 14 9 7
e
Human atrial tissue
SR
AF
kDa
Pro-CT
GAPDH
Pro-CT/GAPDH
P=0.008
SR AF
n= 8 7
f
Pro-CT, pg/ml
P=0.001
SR AF
n= 8 7
g
CT, pg/2x10^4 cells
P=0.0001
SR AF
n=10 8
h
CALCA_mRNA, fc
P=0.02
TT ACM
n= 4 8
i
CT pg/20x10^4 cells, fc
P=0.0008
TT ACM
n= 6 13
k
CALCR_2DCt (relative to RS18)
mRNA
ACF
n = 15
l
[cAMP], nM
EC50=4.9 nM
Vehicle
log [hCT], (M)
n= 4 4 4 4 4 4 4 3 4 4 4
m
cAVP (nM)
P=0.05
P=0.004
P=0.04
ns
calcitonin
PTX
NF499
sCT8-32
FSK
n= 4 6 5 10 10 6 6

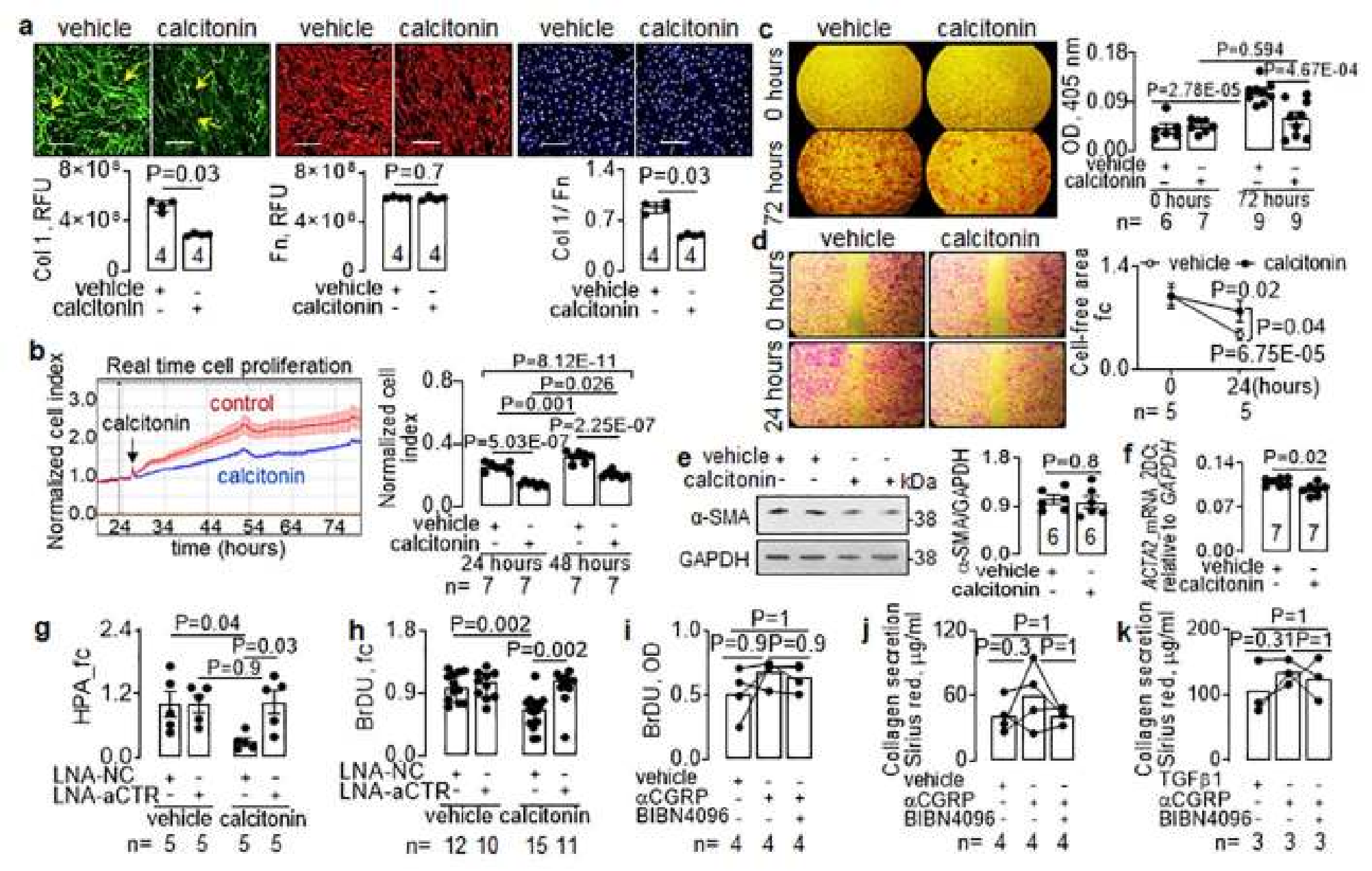
a
vehicle
calcitonin
Col 1, RFU
Fn, RFU
Col 1/ Fn
P=0.03
P=0.7
P=0.03
b
Real time cell proliferation
control
calcitonin
Normalized cell index
time (hours)
P=8.12E-11
P=0.026
P=0.001
P=2.25E-07
P=5.03E-07
24 hours 48 hours
n= 7 7 7 7
c
0 hours
72 hours
OD, 405 nm
P=0.594
P=4.67E-04
P=2.78E-05
n= 6 7 9 9
d
24 hours
Cell-free area fc
P=0.02
P=0.04
P=6.75E-05
n= 5 5
e
α-SMA
GAPDH
kDa
38
α-SMA/GAPDH
P=0.8
f
ACTA2_mRNA_2DC, relative to GAPDH
P=0.02
g
HPA_fc
P=0.04
P=0.03
P=0.9
LNA-NC
LNA-aCTR
n= 5 5 5 5
h
BrDU, fc
P=0.002
P=0.002
n= 12 10 15 11
i
BrDU, OD
P=1
P=0.9 P=0.9
αCGRP
BIBN4096
n= 4 4 4
j
Collagen secretion Sirius red, μg/ml
P=1
P=0.3 P=1
n= 4 4 4
k
P=1
P=0.31 P=1
TGFβ1
n= 3 3 3

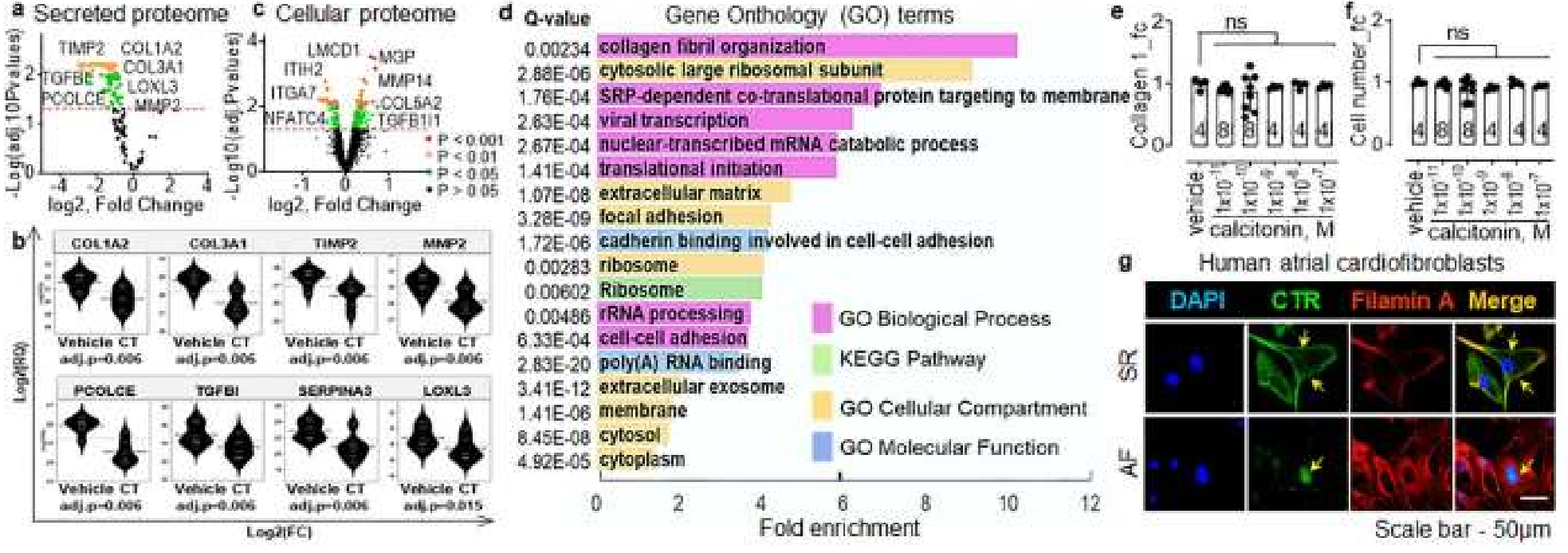
a Secreted proteome
TIMP2
COL1A2
COL3A1
TGFBI
LOXL3
POOLCE
MMP2
-Log(adj.10Pvalues)
log2, Fold Change
c Cellular proteome
LMCD1
MGP
ITIH2
MMP14
ITGA7
COL5A2
NFATC4
TGFB1I1
-Log10(adj.Pvalues)
log2, Fold Change
P < 0.001
P < 0.01
P < 0.05
P > 0.05
b
COL1A2
COL3A1
TIMP2
MMP2
POOLCE
TGFBI
SERPINA3
LOXL3
Vehicle CT
adj.p<0.006
adj.p=0.015
Log2(RIU)
Log2(FC)
d
Q-value
Gene Onthology (GO) terms
0.00234 collagen fibril organization
2.88E-06 cytosolic large ribosomal subunit
1.76E-04 SRP-dependent co-translational protein targeting to membrane
2.63E-04 viral transcription
2.67E-04 nuclear-transcribed mRNA catabolic process
1.41E-04 translational initiation
1.07E-08 extracellular matrix
3.28E-09 focal adhesion
1.72E-06 cadherin binding involved in cell-cell adhesion
0.00283 ribosome
0.00602 Ribosome
0.00486 rRNA processing
6.33E-04 cell-cell adhesion
2.83E-20 poly(A) RNA binding
3.41E-12 extracellular exosome
1.41E-06 membrane
8.45E-08 cytosol
4.92E-05 cytoplasm
GO Biological Process
KEGG Pathway
GO Cellular Compartment
GO Molecular Function
0 2 4 6 8 10 12
Fold enrichment
e
ns
Collagen 1_fc
vehicle
1x10-11
1x10-10
1x10-9
1x10-8
1x10-7
calcitonin, M
f
ns
Cell number_fc
vehicle
1x10-11
1x10-10
1x10-9
1x10-8
1x10-7
calcitonin, M
g
Human atrial cardiofibroblasts
DAPI
CTR
Filamin A
Merge
SR
AF
Scale bar - 50µm

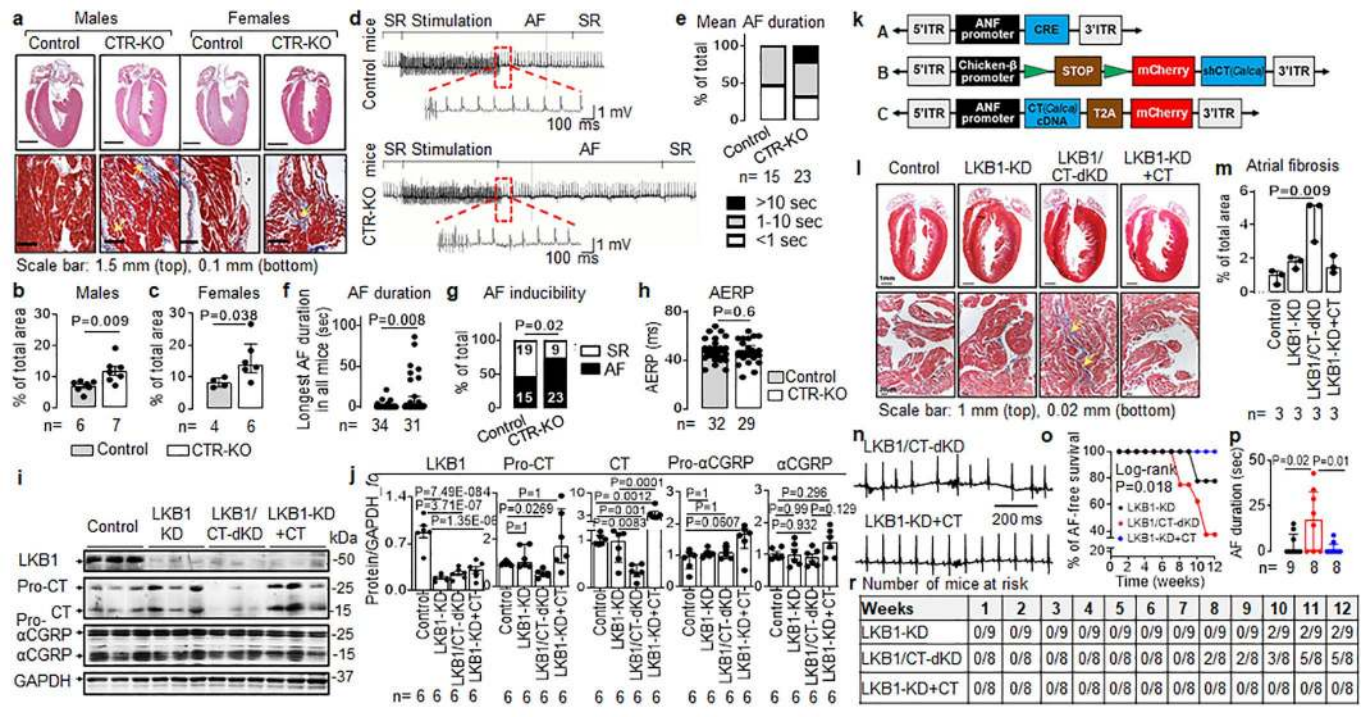
a
Males
Females
Control
CTR-KO
Control
CTR-KO
Scale bar: 1.5 mm (top), 0.1 mm (bottom)
b
Males
% of total area
P=0.009
n= 6 7
Control
CTR-KO
c
Females
% of total area
P=0.038
n= 4 6
f
AF duration
Longest AF duration in all mice (sec)
P=0.008
n= 34 31
g
AF inducibility
% of total
P=0.02
19
9
15
23
SR
AF
Control
CTR-KO
h
AERP
AERP (ms)
P=0.6
n= 32 29
Control
CTR-KO
d
SR Stimulation
AF
SR
Control mice
1 mV
100 ms
CTR-KO mice
e
Mean AF duration
% of total
Control
CTR-KO
n= 15 23
>10 sec
1-10 sec
<1 sec
k
A
5'ITR
ANF promoter
CRE
3'ITR
B
5'ITR
Chicken-β promoter
STOP
mCherry
shCT(Calca)
3'ITR
C
5'ITR
ANF promoter
CT(Calca) cDNA
T2A
mCherry
3'ITR
l
Control
LKB1-KD
LKB1/ CT-dKD
LKB1-KD +CT
Scale bar: 1 mm (top), 0.02 mm (bottom)
m
Atrial fibrosis
% of total area
P=0.009
Control
LKB1-KD
LKB1/CT-dKD
LKB1-KD+CT
n= 3 3 3 3
i
Control
LKB1 KD
LKB1/ CT-dKD
LKB1-KD +CT
kDa
LKB1
Pro-CT
CT
Pro-αCGRP
αCGRP
GAPDH
-50
-25
-15
-25
-15
-37
j
LKB1
Pro-CT
CT
Pro-αCGRP
αCGRP
Protein/GAPDH
P=7.49E-084
P=3.71E-07
P=1.35E-08
P=1
P=0.0269
P=1
P=0.0001
P=0.0012
P=0.001
P=0.0083
P=1
P=1
P=0.0607
P=0.296
P=0.99
P=0.129
P=0.932
Control
LKB1-KD
LKB1/CT-dKD
LKB1-KD+CT
n= 6 6 6 6
n
LKB1/CT-dKD
LKB1-KD+CT
200 ms
o
% of AF-free survival
Log-rank P=0.018
LKB1-KD
LKB1/CT-dKD
LKB1-KD+CT
Time (weeks)
p
AF duration (sec)
P=0.02
P=0.01
n= 9 8 8
r
Number of mice at risk
| Weeks | 1 | 2 | 3 | 4 | 5 | 6 | 7 | 8 | 9 | 10 | 11 | 12 |
|---|---|---|---|---|---|---|---|---|---|---|---|---|
| LKB1-KD | 0/9 | 0/9 | 0/9 | 0/9 | 0/9 | 0/9 | 0/9 | 0/9 | 0/9 | 2/9 | 2/9 | 2/9 |
| LKB1/CT-dKD | 0/8 | 0/8 | 0/8 | 0/8 | 0/8 | 0/8 | 0/8 | 2/8 | 2/8 | 3/8 | 5/8 | 5/8 |
| LKB1-KD+CT | 0/8 | 0/8 | 0/8 | 0/8 | 0/8 | 0/8 | 0/8 | 0/8 | 0/8 | 0/8 | 0/8 | 0/8 |